POAC'25
St. John's, Newfoundland and Labrador, Canada

Proceedings of the 28th International Conference on Port and Ocean Engineering under Arctic Conditions
Jul 13-17, 2025
St. John's, Newfoundland and Labrador
Canada

Research on Ship Path Planning Method in Low Ice Concentration Areas

Yixin Wang[1,2], Xiaodong Chen[1,2], Shunying Ji[1,2]
[1] Dalian University of Technology, Dalian, China
[2] State Key Laboratory of Structural Analysis, Optimization and CAE Software for Industrial Equipment, Dalian, China

ABSTRACT

The complexity and uncertainty of sea ice distribution pose significant challenges for vessel navigation in ice-covered regions. This paper proposes a path planning method specifically designed for low ice concentration areas. By utilizing high-resolution sea ice images captured by the icebreaker *Xue Long 2*, a navigation environment for ice-covered waters is established. Combined with the *Xue Long 2* ship maneuvering model, a two-layer path planning model is developed. The model integrates the Hybrid A* algorithm with optimal control theory and employs a neural network surrogate model to replace the traditional direct collocation method, mitigating the computational burden of excessive optimization variables. Case studies conducted under varying sea ice concentration scenarios demonstrate the method's effectiveness in identifying optimal paths through ice channels, confirming its strong applicability.

KEY WORDS: Arctic Navigation; Path Planning; Hybrid A* Algorithm; Optimal Control; Neural Network

1 INTRODUCTION

With global climate change, the extent of sea ice in the Arctic region has been gradually decreasing, leading to improved navigational conditions and further development of economic activities and resource exploitation in the region (Stephenson et al., 2018). Polar shipping and scientific exploration have gained significant attention (Beveridge et al., 2016). Compared to traditional routes through the Suez Canal, the Arctic Northeast Passage shortens the shipping distance between the Far East and Europe by 30-40% (Lasserre and Pelletier, 2011), and virtually eliminates the risk of piracy. However, due to the unique geographical location and environmental conditions of the Arctic, accidents occurring along the Northeast Passage will have more severe consequences and be harder to respond to in a timely manner

than those on traditional routes. Unlike path planning in open waters, route planning in ice-covered regions requires consideration of the impacts of ice conditions on the vessel (Pastusiak, 2016), as the presence of sea ice significantly affects the safety of vessel navigation (Fu et al., 2016). Therefore, utilizing reliable sea ice information for path planning is a key issue for safe navigation in ice-covered regions.

To date, most studies on ship path planning in ice-covered regions have relied on low-resolution satellite images, weather forecasting data, sea ice model forecasts, and ice charts. Recent advancements have introduced local sea ice path planning algorithms utilizing real-ship radar data (Berglund, Kotovirta, and Seinä, 2007; Lin et al., 2021). Existing path planning models for ships in ice-covered areas primarily focus on the development and integration of three modules: sea ice models, ship navigation models, and optimization algorithms (Li, Ringsberg, and Rita, 2019; Zhang et al., 2019; Chen et al., 2020; Lee, Roh, and Kim, 2021; Mishra et al., 2021; Zvyagina and Zvyagin, 2022; Wu et al., 2022). As vessels move towards automation, more sensors are being installed on ships, enhancing their perception capabilities (Wróbel, Montewka, and Kujala, 2018). Lin et al. (2021) developed a near-field route planner based on ship radar images, which can dynamically and accurately update the route based on sea ice conditions. Currently, most research on path planning in ice-covered regions focuses on global route planning at the satellite remote sensing scale, with little attention given to local path planning at the vessel scale.

In ice-covered regions, commercial vessels typically have low or no ice class and primarily navigate in areas with lower sea ice concentration (Heikkilä et al., 2024). Collisions with sea ice may lead to both speed reduction and potential hull damage, prompting commercial vessels to avoid ice floes whenever possible. Conventional path planning methods and global planning approaches in ice-covered regions are not suitable for local path planning in these areas. To address the problem of path selection for vessels navigating in low sea ice concentration regions, this paper proposes a two-layer path planning model based on images captured by onboard cameras. The Hybrid A* algorithm is used to determine the shorter path in terms of navigation time, and the path obtained from the Hybrid A* algorithm is used as the initial solution for an optimal control problem. The optimal control method is then applied to generate an optimized path that satisfies the vessel's kinematic constraints.

2 METHODOLOGY

2.1 Research Framework

The proposed path planning model framework is shown in Figure 1. High-resolution sea ice images are obtained from the sensors onboard the icebreaker *Xue Long 2*, and an image correction algorithm (Lu and Li, 2010) is applied to recover approximate dimensions of the sea ice. The corrected images are then processed using a deep learning model (Zhang et al., 2022) to identify the distribution of sea water and ice, yielding an array of sea ice positions used for path planning. To ensure that the generated path effectively avoids potential hazardous sea ice and meets the vessel's maneuverability constraints, the ship's maneuvering model is incorporated into the path planning process. Based on this, a two-layer path planner combining the Hybrid A* algorithm with optimal control theory is designed, and a neural network surrogate model is employed to replace the direct collocation method for handling vessel motion constraints, thereby extending the applicability of the established path planning approach.

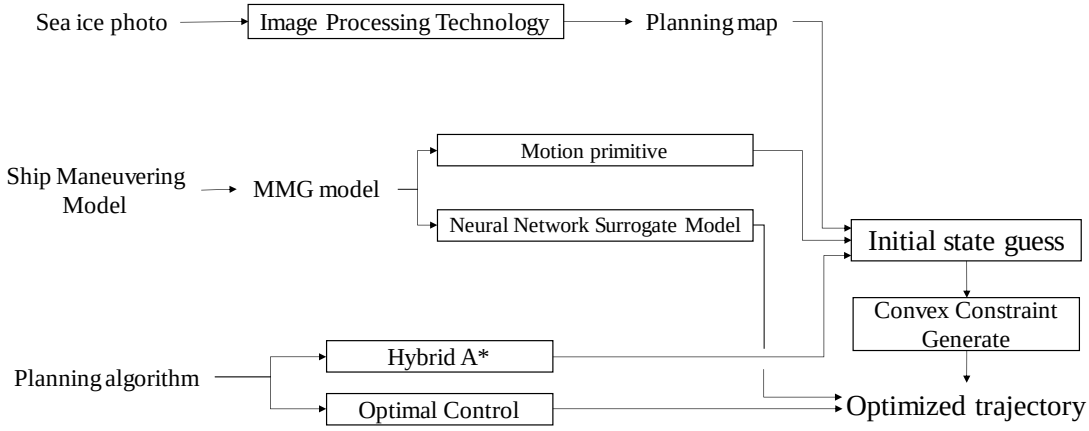

Figure 1. Path Planning Process in Low Ice Concentration

2.2 *Xue Long 2* Maneuvering Model

Due to the highly complex navigation environment in the Arctic region, the shape and distribution of sea ice around the ship's hull are fraught with uncertainty. When planning paths, it is essential to fully consider the dynamic constraints of the vessel to prevent difficulties in tracking the planned path, which could lead to ship-ice collisions causing structural damage or entrapping the ship in ice. Therefore, this study incorporates the MMG (Mathematical Modeling Group) ship maneuvering equations as state constraints in both the Hybrid A* algorithm planning phase and the optimal control problem.

Based on the MMG modular modeling approach, the hull, propeller, and rudder of the *Xue Long 2* are considered separately to establish a three-degree-of-freedom (3-DOF) motion equation system for the vessel. To clearly represent the ship's motion dynamics, this study employs the following inertial and body-fixed coordinate systems to describe the ship's movement, as illustrated in Figure 2.

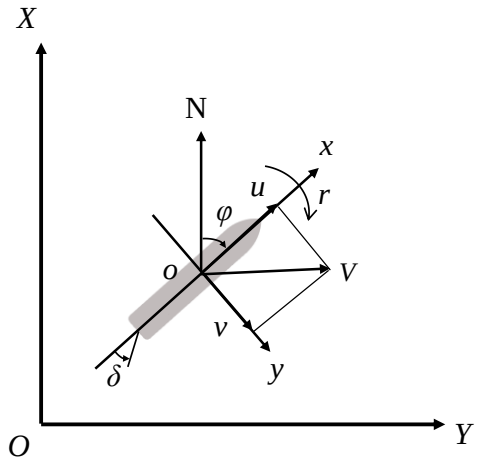

Figure 2. Inertial Reference Frame and Body-Fixed Reference Frame for Ship Motion State

The state vector of the vessel is defined as, $\boldsymbol{x} = [\boldsymbol{\eta}^{\mathrm{T}}\ \boldsymbol{v}^{\mathrm{T}}]^{\mathrm{T}}$, where $\boldsymbol{\eta} = [x\ y\ \varphi]^{\mathrm{T}}$, and $\boldsymbol{v} = [u\ v\ r]^{\mathrm{T}}$. Here, x and y represent the eastward and northward position coordinates of the ship relative to a certain point in the inertial coordinate system, and φ denotes the heading angle of the hull relative to the true north direction. u, v, and r represent the surge velocity, sway velocity, and yaw rate, respectively, in the body-fixed coordinate system. In the body-fixed coordinate

system, the hull is primarily subjected to inertial hydrodynamic forces, viscous hydrodynamic forces, propeller thrust, and rudder forces. The inertial hydrodynamic forces can be modeled as the added mass and added moment of inertia effects of the hull. Consequently, the MMG equations established in the aforementioned coordinate system are as follows:

$$\begin{cases} (m+m_{\mathrm{x}})\dot{u}-(m+m_{\mathrm{y}})rv=\sum X=X_{\mathrm{H}}+X_{\mathrm{P}}+X_{\mathrm{R}} \\ (m+m_{\mathrm{y}})\dot{v}+(m+m_{\mathrm{x}})ru=\sum Y=Y_{\mathrm{H}}+Y_{\mathrm{P}}+Y_{\mathrm{R}} \\ (I_{zz}+J_{zz})\dot{r}=\sum N=N_{\mathrm{H}}+N_{\mathrm{P}}+N_{\mathrm{R}} \\ \dot{x}=u\cos\varphi-v\sin\varphi \\ \dot{y}=v\cos\varphi+u\sin\varphi \\ \dot{\varphi}=r \end{cases} \tag{1}$$

where m denotes the hull's mass, I_{zz} denotes the hull's moment of inertia, and m_{x}, m_{y}, and J_{zz} correspond to the longitudinal added mass, lateral added mass, and added moment of inertia of the hull, respectively. ΣX, ΣY, and ΣN represent the longitudinal external force, lateral external force, and yaw moment acting on the hull in the body-fixed coordinate system. The subscripts H, P, and R denote the viscous hydrodynamic force, propeller thrust, and rudder force, respectively.

In this study, it is assumed that the *Xue Long* 2 operates at rated power continuously, with the ship speed determined by the hydrodynamic forces, rudder forces, and propeller thrust acting on the vessel (Sukas et al., 2019).

2.3 First Stage Planner: Hybrid A* Algorithm

The Hybrid A* (Dolgov et al., 2008) algorithm is an extension of the A* algorithm that incorporates the actual kinematic constraints of the object for path planning. The navigational environment model is constructed as a 2D grid with a resolution of 450m (15 pixels) per cell. The starting point is set at the vessel's photographed location, while the destination is defined as the nearest ice-free area within a 15-kilometer range directly ahead of the ship. The state variable $\boldsymbol{x}_k = [\boldsymbol{\eta}_k^{\mathrm{T}}\ \boldsymbol{v}_k^{\mathrm{T}}]^{\mathrm{T}}$, represents the state at the k-th discrete time step, where $\boldsymbol{\eta}_k$ denotes the position and orientation, and $\boldsymbol{v}_k$ represents the velocity components. The control variable $\boldsymbol{u}_k = [\delta_k]$ represents the control input, specifically the rudder angle. The cost function associated with the state variable $\boldsymbol{x}_k$ is defined as follows:

$$J(\mathbf{x}_k,\mathbf{u}_k)=\min_{\{\mathbf{u}_i\}_{i=1}^{k}}\Big(\sum_{i=1}^{k}c_1\int_{t_{i-1}}^{t_i}\sqrt{u(t)^2+v(t)^2}\,dt+c_2\frac{\delta_i}{k}\Big)+c_3H(\mathbf{x}_k) \tag{2}$$

Where $H(\boldsymbol{x}_i)$ represents the heuristic cost generated by the Dijkstra algorithm. The cost function incorporates three penalty coefficients where c_1 represents the distance penalty term, c_2 denotes the steering penalty term, and c_3 weights the heuristic function. A larger c_3 value accelerates the Hybrid A* algorithm's pathfinding process. This study sets c_1=1.5, c_2=1, and c_3=5.

The dynamic constraints acting on the vessel, $\boldsymbol{x}_{k+1} = f(\boldsymbol{x}_k,\boldsymbol{u}_k)$, are derived from the discretized ship maneuvering equations described in Section 2.2. In this study, motion primitives are generated by varying the rudder angle and limiting the change in the heading angle. To ensure continuity between motion primitives, i.e., $\boldsymbol{v}_k = \boldsymbol{v}_{k-1}$, the rudder is only actuated during the initial period of each motion primitive, while the rudder angle remains zero for the remaining time. As a result, the terminal state of each motion primitive only includes the surge velocity,

which corresponds to the steady-state speed. The motion primitives used in this study are illustrated in Figure 3, where eleven action strategies are defined for both left and right rudder angles, as summarized in Table 1. The algorithm initiates from the starting state $\boldsymbol{x}_0$ and propagates through state transitions via motion primitives. At each iteration, the cost function $J(\boldsymbol{x}_k, \boldsymbol{u}_k)$ evaluates all feasible transitions, expanding the path with the minimal accumulated cost.

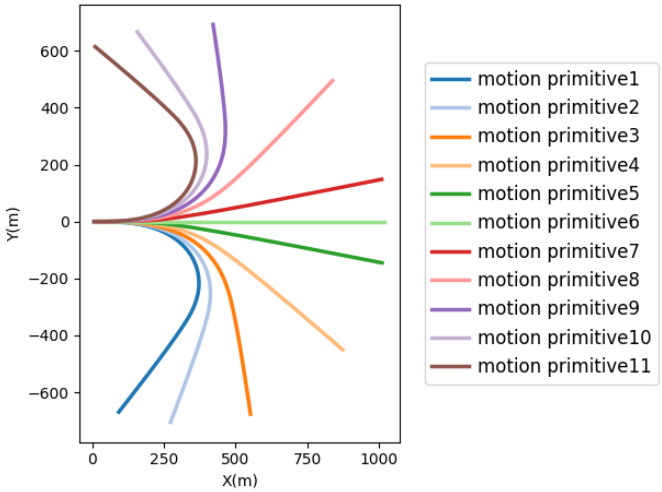

Figure 3. Motion primitives under different steering strategies

Table 1. Motion primitive parameters

No.	Rudder angle(°)	Length（m）	No.	Rudder angle(°)	Length（m）
01	20	1024	07	-4	1024
02	16	1023	08	-8	1022
03	12	1023	09	-12	1022
04	8	1021	10	-16	1023
05	4	1025	11	-20	1021
06	0	1022			

2.4 Second Stage Planner: Optimal Control

The paths generated by the Hybrid A* algorithm are kinematically feasible. Using these Hybrid A*-generated paths as initial solutions significantly accelerates the solving speed of the optimal control problem. Given the complex shapes and distribution patterns of sea ice obstacles, this study employs a convex constraint generation method (Bitar et al., 2020) capable of handling arbitrarily shaped sea ice obstacles, which converts non-convex sea ice constraints into convex constraints to improve optimal control solution efficiency.

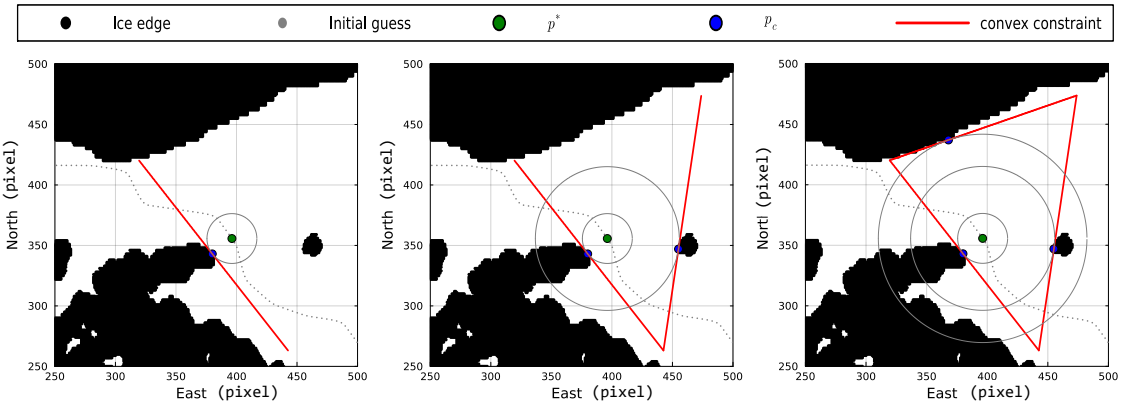

Figure 4. Convex Constraint Generation Pipeline for Sea Ice Obstacles

The constraint generation process is illustrated in Figure 4. The convex polygon constraint generation algorithm proceeds iteratively for each waypoint $\boldsymbol{p}_k = [x_k\ y_k]^{\mathrm{T}}$ along the initial path: taking the initial path waypoint $\boldsymbol{p}_k = [x_k\ y_k]^{\mathrm{T}}$ as the center, we iteratively expand a circle until it intersects with the sea ice pixel at point $\boldsymbol{p}_{\mathrm{c},k,1}$. A tangent line is then constructed at $\boldsymbol{p}_{\mathrm{c},k,1}$, and the circle continues expanding until the next intersection with the sea ice pixel, where another tangent line is drawn. This process repeats until all tangent lines form a closed convex polygon.

The path waypoints $\boldsymbol{p}$ are constrained within the generated convex regions through contact points $\boldsymbol{p}_{\mathrm{c}}$. The ship's state constraints can be mathematically expressed as follows:

$$\underbrace{\begin{bmatrix} \dfrac{(\mathbf{p}_{\mathrm{c},k,1}-\mathbf{p}_k^*)^T}{\left\|\mathbf{p}_{\mathrm{c},k,1}-\mathbf{p}_k^*\right\|_2} \\ \dfrac{(\mathbf{p}_{\mathrm{c},k,2}-\mathbf{p}_k^*)^T}{\left\|\mathbf{p}_{\mathrm{c},k,2}-\mathbf{p}_k^*\right\|_2} \\ \cdots \\ \dfrac{(\mathbf{p}_{\mathrm{c},k,m}-\mathbf{p}_k^*)^T}{\left\|\mathbf{p}_{\mathrm{c},k,m}-\mathbf{p}_k^*\right\|_2} \end{bmatrix}}_{\mathbf{A}_k} \mathbf{p} \le \underbrace{\begin{bmatrix} \dfrac{(\mathbf{p}_{\mathrm{c},k,1}-\mathbf{p}_k^*)^T\mathbf{p}_{\mathrm{c},k,1}}{\left\|\mathbf{p}_{\mathrm{c},k,1}-\mathbf{p}_k^*\right\|_2} \\ \dfrac{(\mathbf{p}_{\mathrm{c},k,2}-\mathbf{p}_k^*)^T\mathbf{p}_{\mathrm{c},k,2}}{\left\|\mathbf{p}_{\mathrm{c},k,2}-\mathbf{p}_k^*\right\|_2} \\ \cdots \\ \dfrac{(\mathbf{p}_{\mathrm{c},k,m}-\mathbf{p}_k^*)^T\mathbf{p}_{\mathrm{c},k,m}}{\left\|\mathbf{p}_{\mathrm{c},k,m}-\mathbf{p}_k^*\right\|_2} \end{bmatrix}}_{\mathbf{b}_k} - r \tag{3}$$

The discrete optimal control problem is described as follows:

$$\begin{aligned} \min_{\mathbf{u}_{1:N-1}} \quad & J = \sum_{i=1}^{N-1}\sqrt{(x_{i+1}-x_i)^2+(y_{i+1}-y_i)^2} \\ \text{subject to } & \mathbf{C}(\mathbf{x}_k,\mathbf{u}_k,\mathbf{x}_{k+1},\mathbf{u}_{k+1})=0 \\ & \mathbf{A}_k[x_k \quad y_k]^T-\mathbf{b}_k-r\le 0 \\ & \mathbf{u}_{lb}\le\mathbf{u}_k\le\mathbf{u}_{ub} \quad k=1,\ldots,N-1 \\ & \mathbf{x}_1=\mathbf{x}_{\text{start}} \\ & \mathbf{x}_N=\mathbf{x}_{\text{goal}} \end{aligned} \tag{4}$$

The state constraint equation $\boldsymbol{C}(\boldsymbol{x}_k,\boldsymbol{u}_k,\boldsymbol{x}_{k+1},\boldsymbol{u}_{k+1})=0$ represents the ship's dynamic equation (Equation 1). Due to the large-scale planning problem, directly using Hybrid A* path points

as initial solutions would lead to excessive problem dimensionality. The proposed solution involves:

1. Reducing the number of initial path points
2. Increasing the time step between adjacent points

With larger time steps, the direct collocation method becomes unsuitable. This study employs a neural network to approximate the ship's dynamic equations, enabling motion prediction at arbitrary time steps (network architecture shown in Figure 5). Given the previous state $\boldsymbol{\eta}_k$, the subsequent state $\boldsymbol{x}_{k+1}$ depends solely on $\boldsymbol{v}_k$ and $\boldsymbol{u}_k$, which serve as network inputs, with $\boldsymbol{x}_{k+1}$ computed via Equation 5.

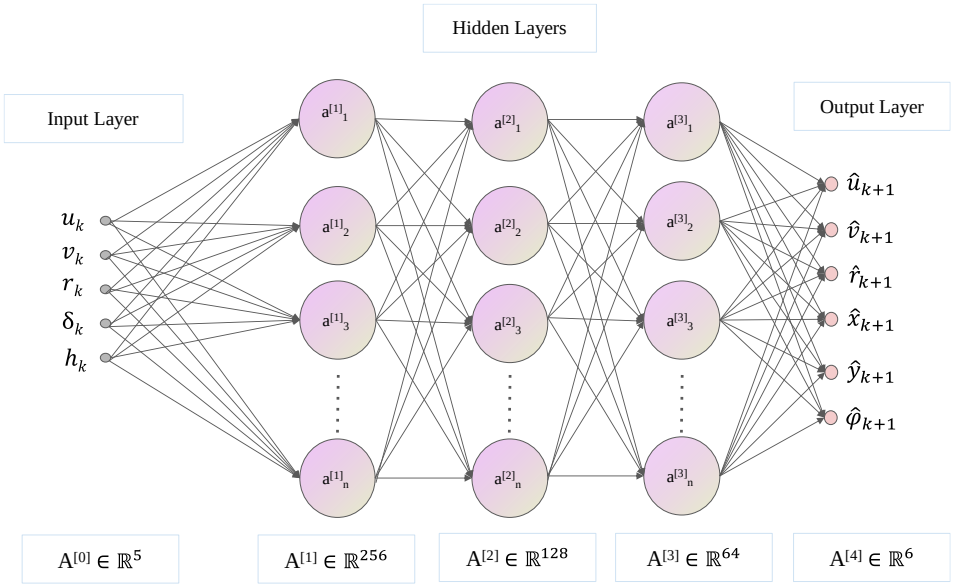

Figure 5. Neural Network Surrogate Model

Training data is generated using the *Xue Long 2* maneuvering equations established in Section 2.2, with the optimization problem ultimately solved using the Ipopt solver.

$$\begin{cases} u_{k+1} = \hat{u}_{k+1} \\ v_{k+1} = \hat{v}_{k+1} \\ r_{k+1} = \hat{r}_{k+1} \\ x_{k+1} = x_k + \sqrt{\hat{x}_{k+1}{}^2 + \hat{y}_{k+1}{}^2}\cos(\hat{\varphi}_{k+1} + \tan^{-1}\dfrac{\hat{y}_{k+1}}{\hat{x}_{k+1}}) \\ y_{k+1} = y_k + \sqrt{\hat{x}_{k+1}{}^2 + \hat{y}_{k+1}{}^2}\sin(\hat{\varphi}_{k+1} + \tan^{-1}\dfrac{\hat{y}_{k+1}}{\hat{x}_{k+1}}) \\ \varphi_{k+1} = \varphi_k + \hat{\varphi}_{k+1} \end{cases} \tag{5}$$

3 RESULTS AND DISCUSSION

In this section, we apply the path planning model described in Section 2 to conduct case studies for sea ice scenarios with different sea ice concentrations (SIC). Note that these case studies are designed to demonstrate the model's performance in low-concentration ice regions.

As the calibration of sea ice map parameters remains a subject for future research, uncalibrated sea ice map parameters were used in these case studies.

This study selects sea ice images captured by the *Xue Long 2* vessel as baseline scenarios. Three scenarios with ice concentrations of 7.5%, 20.6%, and 33% were selected (Figure 6). The planning domain covers a rectangular area of 21 km (east-west) × 15.9 km (north-south). The path planning model established in Section 2 was tested under these different scenarios. Smaller ice floes have been filtered out, meaning all sea ice shown on the map must be avoided by the vessel.

As can be seen from Figure 6, the Hybrid A* algorithm is capable of finding collision-free paths that satisfy the ship's kinematic constraints in complex ice fields. However, since the algorithm searches in a discretized state space, the optimality of the generated paths cannot be guaranteed. Moreover, the algorithm involves numerous parameters, making it difficult to further improve path quality through parameter tuning.

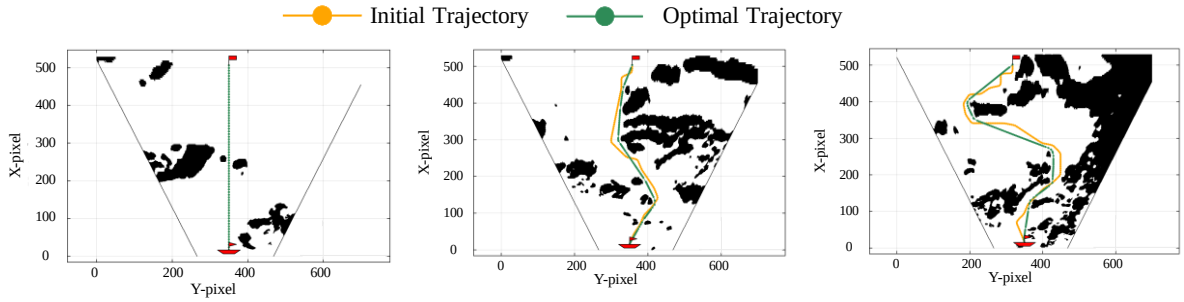

(a)case1 SIC=7.5% (b)case2 SIC=20.6% (c)case3 SIC=33%

Figure 6. Path Planning Results

Table 2 presents the performance metrics of the path planning results. The mean heading change is obtained by calculating the average of absolute heading angle variations at each time step, reflecting the frequency of course adjustments, while the mean rudder angle represents the average of absolute rudder angles at each time step, characterizing the steering intensity.

Table 2. Path Planning Performance Metrics

Case	Hybrid A* Algorithm			Optimal Control Solver		
	Length (m)	Mean Heading Change(°)	Mean Rudder Angle(°)	Length (m)	Mean Heading Change(°)	Mean Rudder Angle(°)
01	15000	0	0	15000	0	0
02	19800	25.0	11.1	16255	1.9	4.8
03	29700	27.0	10.4	21750	2.7	5.0

For Case 1, the path obtained by the Hybrid A* algorithm is already optimal, as evidenced by the fact that no changes occurred after optimal control-based replanning. This demonstrates that the Hybrid A* algorithm can indeed find optimal paths under specific conditions. For other cases, the paths generated by the optimal control method are smoother and shorter compared to those from the Hybrid A* algorithm.

The case studies prove that the proposed two-layer path planning model exhibits good applicability across scenarios with different sea ice concentrations. The developed hierarchical planning method can not only effectively handle complex low-concentration ice conditions but also enhance path planning safety while respecting the ship's actual maneuvering constraints.

It should be noted that the current study focuses solely on low-concentration ice regions. Future work should incorporate ship-ice interaction mechanisms to improve the model's generalizability.

4 CONCLUSIONS

This paper proposes a two-layer path planning model based on Hybrid A* algorithm and optimal control theory to address ship path planning in low-concentration ice-covered waters. During the path optimization process, special attention is given to the dynamic constraints of the vessel. The research demonstrates that this model can integrate high-resolution ice image captured by onboard cameras with ship kinematic constraints to generate safe, smooth, and maneuverability-compliant optimized paths in various ice-covered environments.

While the current path planning model has been numerically validated, its performance will be further evaluated in polar-like environments. Subsequent development will integrate ship-ice interaction modeling to address icebreaking navigation in high-density ice conditions.

ACKNOWLEDGEMENTS

This research was supported by the National key research and development program (Grant No. 2024YFC2816403), National Natural Science Foundation of China (Grant Nos. 52101300,52192693, 52192690, 42176241), Social Development Science and Technology Project of Shanghai Science and Technology Innovation Plan (22DZ1204500) and Special Project of Ministry of Industry and In-formation Technology of China (Grand No. 2021-342).

REFERENCES

Berglund, R., Kotovirta, V., & Seinä, A., 2007. A system for icebreaker navigation and assistance planning using spaceborne SAR information in the Baltic Sea, *Canadian Journal of Remote Sensing*, 33, 378-87.

Beveridge, L., Fournier, M., Lasserre, F., Huang, L., & Têtu, P.L., 2016. Interest of Asian shipping companies in navigating the Arctic, *Polar Science*, 10, 404-414.

Bitar, G., Martinsen, A.B., Lekkas, A.M., & Breivik M., 2020. Two-Stage Optimized Trajectory Planning for ASVs Under Polygonal Obstacle Constraints: Theory and Experiments, *IEEE Access*, 8, 199953-69.

Chen, X., Sheti, W., Li, H., Cui, Y., Luo, Z., & Li, J., 2020. Ship Navigation Route Planning Using Topology of Sea Ice Channels Extracted from High Resolution Satellite Images, In: *IGARSS 2020 - 2020 IEEE International Geoscience and Remote Sensing Symposium*, 3066-69.

Dolgov, D., Thrun, S., Montemerlo, M., & Diebel, J., 2008. Practical search techniques in path planning for autonomous driving, In: *Proceedings of the First International Symposium on Search Techniques in Artificial Intelligence and Robotics*, STAIR-08.

Fu, S., Zhang, D., Montewka, J., Yan, X., & Zio, E., 2016. Towards a probabilistic model for predicting ship besetting in ice in Arctic waters, *Reliability Engineering & System Safety*, 155, 124-36.

Heikkilä, M., Grönholm, T., Majamäki, E., Jalkanen, J.P., 2024. Effect of ice class to vessel fuel consumption based on real-life MRV data, *Transport Policy*, 148, 168-180.

Lasserre, F., & Pelletier, S., 2011. Polar super seaways? Maritime transport in the Arctic: an analysis of shipowners' intentions, J*ournal of Transport Geography*, 19, 1465-73.

Lee, H.W., Roh, M.I., & Kim, K.S., 2021. Ship route planning in Arctic Ocean based on POLARIS, *Ocean Engineering*, 234, 109297.

Li, Z., Ringsberg, J.W., & Rita, F.A., 2019. A Voyage Planning Tool for Arctic Transit of Cargo Ships, In: *ASME 2019 38th International Conference on Ocean, Offshore and Arctic Engineering*, OMAE2019-95128.

Lin, X., Wang, S., Zhang, X., Hsieh, T.H., Sun, Z., & Xu, T. 2021. Near-Field Route Optimization-Supported Polar Ice Navigation via Maritime Radar Videos, *Journal of Advanced Transportation*, 2021, 2798351.

Lu, P., & Li, Z., 2010. A Method of Obtaining Ice Concentration and Floe Size From Shipboard Oblique Sea Ice Images. *IEEE Transactions on Geoscience and Remote Sensing* , 48, 2771-2780.

Mishra, P., Alok, S., Rajak, D.R., Beg, J.M., Bahuguna, I.M., & Talati, I., 2021. Investigating optimum ship route in the Antarctic in presence of sea ice and wind resistances – A case study between Bharati and Maitri, *Polar Science*, 30, 100696.

Pastusiak, T., 2016. Principles of Vessel Route Planning in Ice on the Northern Sea Route, *TransNav, the International Journal on Marine Navigation and Safety of Sea Transportation*, 10, 587-92.

Stephenson, S.R., Wang, W., Zender, C.S., Wang, H., Davis, S.J., & Rasch P.J., 2018. Climatic Responses to Future Trans-Arctic Shipping, *Geophysical Research Letters*, 45, 9898-908.

Sukas, O. F., Kinaci, O.K., Bal, 2019. Theoretical background and application of MANSIM for ship maneuvering simulations, *Ocean Engineering*, 192, 106239.

Wróbel, K., Montewka, J., & Kujala, P., 2018. System-theoretic approach to safety of remotely-controlled merchant vessel, *Ocean Engineering*, 152, 334-45.

Wu, A., Che, T., Li, X., & Zhu, X., 2022. Routeview: an intelligent route planning system for ships sailing through Arctic ice zones based on big Earth data. *International Journal of Digital Earth*, 15, 1588-613.

Zhang, C., Zhang, D., Zhang, M., & Mao, W., 2019. Data-driven ship energy efficiency analysis and optimization model for route planning in ice-covered Arctic waters. *Ocean Engineering*, 186, 106071.

Zhang, C., Chen, X., Ji, S., 2022, Semantic image segmentation for sea ice parameters recognition using deep convolutional neural networks, *International Journal of Applied Earth Observation and Geoinformation* ,112, 102885.

Zvyagina, T., & Zvyagin, P., 2022. Finding Risk-Expenses Pareto-Optimal Routes in Ice-Covered Waters. *Journal of Marine Science and Engineering*, 10(7), 862.